Open access • Journal Article • DOI:10.1039/C3TC32116A

Synthesis and evaluation of a PVDF–PT3MA–Zn2SiO4:Mn hybrid polymeric composite for optical device applications — Source link

Alex Linardi Gomes, Alex Linardi Gomes, Rossano Lang, Elaine Armelin ...+2 more authors

Institutions: Polytechnic University of Catalonia, State University of Campinas, Federal University of São Paulo

Published on: 13 Mar 2014 - Journal of Materials Chemistry C (The Royal Society of Chemistry)

Topics: Inorganic compound, Photoluminescence, Scanning electron microscope and Luminescence

Journal of Materials Chemistry C

PAPER

View Article Online
View Journal | View Issue

Cite this: J. Mater. Chem. C, 2014, 2, 2502

Synthesis and evaluation of a PVDF–PT3MA–Zn_2SiO_4:Mn hybrid polymeric composite for optical device applications

Alex Linardi Gomes,[ab] Rossano Lang,*[c] Elaine Armelin,[bd] Carlos Alemán[bd] and João Sinezio de Carvalho Campos[a]

A new hybrid organic/inorganic composite consisting of poly(3-thiophene methyl acetate) (PT3MA), poly(vinylidene fluoride) (PVDF) and manganese-doped zinc silicate (Zn_2SiO_4:Mn) has been synthesized and applied for the fabrication of an optical device. Recrystallized PVDF was used as a host matrix for the PT3MA polymer and Zn_2SiO_4:Mn inorganic compound. The active layer was deposited on an indium-tin-oxide (ITO)-coated glass substrate by the drop casting technique. A spin-coating method was also used for morphological comparison purposes. The synthesized material as well as the device (aluminium electrodes/PVDF–PT3MA–Zn_2SiO_4:Mn/ITO/glass) was characterized by scanning electron microscopy (SEM), atomic force microscopy (AFM), energy dispersive X-ray spectroscopy (EDX), dark current–voltage (*I–V*) characteristic curves, absorbance and photoluminescence (PL) spectroscopy. The results show spherical- and irregular-shaped microparticles both dispersed on and within the PVDF matrix, which correspond to PT3MA and Zn_2SiO_4:Mn, respectively. The hybrid composite shows strong luminescence at ≈525 nm superimposed by a broadband between 600 and 800 nm, originating from the Zn_2SiO_4:Mn radiative transitions and from the recombination of photogenerated carriers at PT3MA. At room temperature, the device presented semiconductor behaviour typically observed for photodetectors and a DC electrical conductivity of ≈0.37 μS cm^{-1}.

Received 26th October 2013
Accepted 15th January 2014

DOI: 10.1039/c3tc32116a

www.rsc.org/MaterialsC

Introduction

Hybrid organic/inorganic composites are appealing alternatives for a great diversity of systems and electro-optical applications.[1–3] Semiconducting polymers combined with inorganic compounds of different nature can generate a variety of new materials with interesting and unique additional physical properties. Some exciting demonstrations have been reported recently. In the field of optoelectronics, hybrid organic/inorganic light-emitting devices (HyLEDs) are emerging as promising candidates for next-generation solid-state lighting sources because of their excellent properties of low-power consumption, high mechanical flexibility and chemical structural versatility.[4–6] Particularly, HyLEDs containing inorganic phosphor such as manganese-doped zinc silicate have attracted considerable attention due to their high light extraction efficiency.[7–9] Mn-doped Zn_2SiO_4 is a well-known green emitting phosphor, which has been applied in many industrial fields such as plasma and flat display panels, fluorescent lamps, cathode-ray tubes and light-emitting devices.[10–13]

Hybrid photovoltaic[14–17] and photodetector[18–21] devices have also been a subject of research. Devices with better detection and remarkably broader spectral response than those of purely inorganic counterparts have been demonstrated.[20,21] From this point of view, the study and the development of new hybrid polymeric composites would be of interest to explore potential properties suitable for application in advanced optical components.

Among organic conducting polymers, polythiophene and its derivatives are important technological materials because of their good electrical conductivity, electroluminescence, and nonlinear optical properties, as well as excellent solubility and processability.[22–26] However, polythiophenes have poor mechanical properties such as low flexibility, but that could be improved by mixing with other polymers like poly(vinylidene fluoride) (PVDF). PVDF is an insulating fluorinated polymer with good mechanical properties and it, in principle, can provide flexibility, stability and easy moldability.[27,28] Therefore, nanostructured polythiophenes in the PVDF matrix may result in interesting properties. Both are low-cost polymers and can be used as alternative materials for the design and fabrication of

[a]Department of Materials Engineering and Bioprocess, State University of Campinas – UNICAMP, 13083-852, Campinas, SP, Brazil
[b]Departament d'Enginyeria Química, E.T.S d'Enginyers Industrials de Barcelona, Universitat Politècnica de Catalunya, Barcelona E-08028, Spain
[c]Institute of Science and Technology, UNIFESP, 12231-280, São José dos Campos, SP, Brazil. E-mail: rossano.lang@unifesp.br
[d]Center for Research in Nano-Engineering, Universitat Politècnica de Catalunya, Campus Sud, Barcelona E-08028, Spain

electronic devices. Recently, we have carried out detailed studies on the chemical, structural, thermal and electronic properties of the poly(3-thiophene methyl acetate) (PT3MA) polymer and its blends and PT3MA in the PVDF matrix.[29–32] In these studies, the PT3MA chains were doped with ferric chloride ($FeCl_3$).[33,34]

This work reports the material synthesis, fabrication and characterization (morphological, electrical and optical) of a device based on a (PVDF–$FeCl_3$-doped PT3MA–Zn_2SiO_4:Mn) hybrid polymeric composite. At room temperature, the device presented semiconductor behaviour typically observed for photodetectors and the composite exhibited strong luminescence at ≈525 nm superimposed by a broadband between 600 and 800 nm. The active layer was deposited on an indium-tin-oxide (ITO)-coated glass substrate by the drop casting technique using dimethylformamide (DMF) as a solvent. A spin-coating method was also used for comparison purposes. Ohmic electrical contacts were formed by aluminium deposition on the polymer composite surface. Surface morphologies, sizes and shapes of the structures were analysed by scanning electron microscopy (SEM) while the roughness and the thickness average of the polymeric layers were evaluated by atomic force microscopy (AFM) and profilometry, respectively. Cross-section microscopy by focused ion beam (FIB-SEM) was used to obtain internal structural information from the composite layer. The local chemical composition was determined by qualitative microanalyses through energy dispersive X-ray spectroscopy (EDX). The DC electrical conductivity was extracted from current–voltage (*I–V*) characteristic curves. Finally, the optical properties of absorption and light emission were investigated by absorbance and photoluminescence (PL) spectroscopy.

Experimental

Materials, reagents and solvents

3-Thiophene acetic acid (T3AA) monomer and ferric chloride ($FeCl_3$) oxidant used for the nanostructured PT3MA synthesis (Scheme 1), as well as the Zn_2SiO_4:Mn and ITO/glass substrates (with a sheet resistivity of 20 Ω per square), were purchased from Sigma-Aldrich S.A. Dimethylformamide (DMF), acetone, methanol, isopropyl alcohol and sulphuric acid employed in preparations and syntheses were acquired from Labsynth Ltd. The insulating polymer, Kynar 740 (PVDF) in pellets, was donated by Arkema Inc. The aluminium utilized as the electrical contact layer (electrodes) was CERAC AM-104.

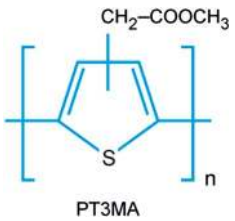

PT3MA

Scheme 1 Chemical structure of poly(3-thiophene methyl acetate) (PT3MA).

Syntheses and preparation of the solutions

Esterification and polymerization reactions of the T3AA monomer were performed by following the procedures suggested by Sugimoto and Osada.[35,36] We have recently reported the complete characterization of the resulting conducting polymer – PT3MA.[30,31]

The hybrid organic/inorganic composite was prepared by keeping the PVDF–PT3MA–Zn_2SiO_4:Mn ratio as 80 : 20 : 80, w/w/w. A typical solution preparation can be described as follows: 40 mg of PVDF in pellets were transferred to a glass flask and completely dissolved in 8 mL of DMF at 90 °C. In a separate glass flask, 10 mg of anhydrous $FeCl_3$-doped PT3MA were added to 2 mL of DMF and heated at 40 °C until full dissolution. Then, the solutions were mixed (completely homogenized) resulting in an initial polymeric solution with 5 mg mL^{-1} concentration. It was then poured into a flask together with 40 mg of Zn_2SiO_4:Mn and kept under stirring at 50 °C for 12 hours. Under such conditions, the PVDF polymer recrystallizes with the microparticles of the inorganic component dispersed into the colloidal solution. The adhesion of the composite onto the ITO film is provided by the polar substituent of PT3MA.

Partial removal of the ITO film and cleaning

Before the depositions of the active layer and of the aluminium electrical contacts, the ITO film was partially removed from the glass plate surface (Fig. 1a and b). The procedures used for the surface preparation were similar to those implemented by Bradshaw[37] and Kim:[38] the glass plate (2.5 cm × 2.5 cm × 1.1 mm) containing the ITO film (nominal ≈ 250 nm) was partially covered with tape and the remaining surface being coated with enamel. After removing the tape, the plate was placed into a glass flask containing HCl solution and Zn powder, and kept for 15 minutes in an ultrasonic bath. The unprotected ITO region was removed by chemical etching (chemical redox reaction). Subsequently, the plates were subjected to a three-step cleaning process in order to eliminate possible contaminants which could affect device performance: acetone (enamel removal), isopropyl alcohol at 70 °C and deionized water for a period of 15 minutes under ultrasound.

Active layer formation

The drop casting technique was used to deposit the hybrid composite onto the chemically cleaned ITO/glass substrate

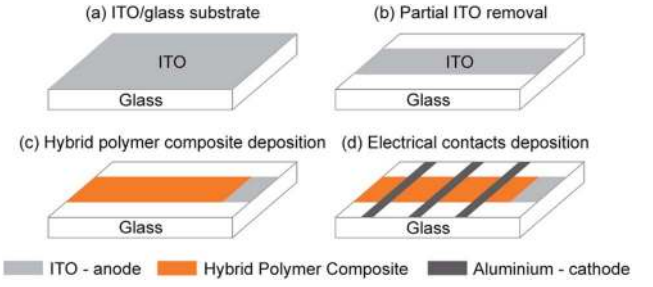

Fig. 1 Schematic illustration of the fabricated device. (a) ITO/glass substrate. (b) Partial removal of the ITO film. (c) Deposition of the hybrid polymeric composite. (d) Deposition of the electrical contacts.

(Fig. 1c). It was also deposited by a spin-coating method at 2000 rpm for comparison purposes. The samples were placed in a forced-air recirculation drying oven where the DMF solvent was evaporated at 90 °C. Later, they were stored in a vacuum desiccator.

Electrical contact deposition by thermal evaporation

Ohmic electrical contacts, with thicknesses of ≈0.5 μm, were formed by Al deposition on the polymer surface by high vacuum thermal evaporation using a coating system (E306A, Edwards). Physical masks made of acrylic resin were placed onto the sample surface before evaporation to delimit the Al deposition area (conductive tracks – Fig. 1d). As a result, parts of the conductive tracks were adhered directly onto the glass after depositions. These track parts serve as contact pads, where one of the tips of the electrical measuring equipment is positioned. The other is on uncovered ITO. The aim is to avoid perforations of the polymeric layer and some short-circuit by the direct contact between the electrodes of the device that arise by burying tips.

After (i) partial ITO removal and cleaning, (ii) preparation of the polymeric solutions and colloid formation, (iii) deposition onto the substrate and (iv) contact metallization, the fabricated device comprised the following heterostructure: Al/PVDF–PT3MA–Zn_2SiO_4:Mn/ITO/glass. The surface area of the device was about 4 cm^2.

Structural, electrical and optical characterizations

Plan-view SEM observations and chemical composition analyses were performed using a high-resolution SEM system (440i LEO Electron Microscopy/Oxford – operated at an accelerating voltage of 20 kV) with an energy dispersive X-ray spectroscopy analyser (EDX) integrated (detector 7060, Oxford). A cross-sectional microscopy image by SEM was acquired using a dual beam FIB-SEM system (Nova NanoLab 200, FEI). A profilometer (Veeco Dektak 6M Stylus) was used to measure the film thicknesses. AFM analyses were performed on a scanning probe microscope (NT-MDT Solver P47 PRO) in semi-contact mode. The DC electrical conductivity measurements (current–voltage characteristic curves) were done using a semiconductor characterization system (Keithley 4200-SCS) as the voltage source and a dynamic signal analyser (Hewlett-Packard 35660A) for the data acquisition. Optical absorption data at room temperature were obtained with a UV-Vis-NIR spectrophotometer (VARIAN Cary 5G). Photoluminescence (PL) spectroscopy measurements at 7 and 295 K were carried out in a continuous flow variable temperature optical He cryostat. The 442 nm line of a He–Cd laser (IK5751I-G, Kimmon Koha) was employed as a photoexcitation source, with an estimated excitation power density of 250 μW mm^{-2}. The PL signal was dispersed using a single monochromator (Spectrapro 2500i with 0.5 m focal length and 1200 g mm^{-1} grating blazed at 550 nm, Princeton Instruments) and detected using a GaAs photomultiplier tube (Hamamatsu) in the 350–850 nm wavelength range. The entrance and exit slits were kept at 150 μm. A long-pass edge filter (442 nm) was also used to eliminate undesired scattering in the monochromator. The PL spectra were corrected for the overall spectral response of the experimental set up.

Results and discussion

For SEM observations and EDX microanalysis, the sample surface was covered with a 100 Å Au film in a sputter coater (SC 7620, Polaron Instruments) to avoid electrostatic charging. The Au coating not only makes the surfaces electrically conductive but also simultaneously prevents material loss from radiation damage during analysis since SEM uses electrons to scan the surface.

Fig. 2 shows representative plan-view SEM images of the composite surface deposited by drop casting technique on the ITO/glass substrate. As can be noticed (Fig. 2a), sphere-like particles and irregular-shaped microstructures (indicated by the arrows) are dispersed on the PVDF matrix, which consists of spherulites[39] with diameter sizes from 7 to 13 μm. Moreover, small pores are also observed, indicating that the evaporation rate of the DMF solvent and the PVDF crystallization were suitable for the polymeric film formation. In this case, the thickness of the film obtained after evaporation of the solvent at 90 °C was 14 μm (average value evaluated by profilometry). A SEM micrograph at higher magnification (Fig. 2b) shows the sphere-like particles (average diameters from 1.3 to 2.2 μm) and the PVDF spherulites in detail.

The local elemental chemical composition was determined by EDX microanalyses. Qualitative results are shown in the spectra of Fig. 3. The EDX line scanning across sphere-like

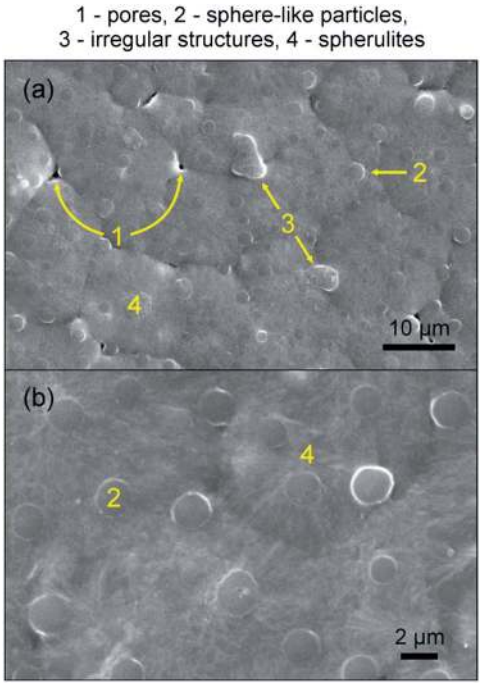

Fig. 2 SEM micrographs of the hybrid polymeric composite surface prepared by the drop casting technique showing: (a) sphere-like particles and irregular-shaped microstructures dispersed on the PVDF matrix – which consists of spherulites, besides the small pores. (b) Sphere-like particles and PVDF spherulites in detail.

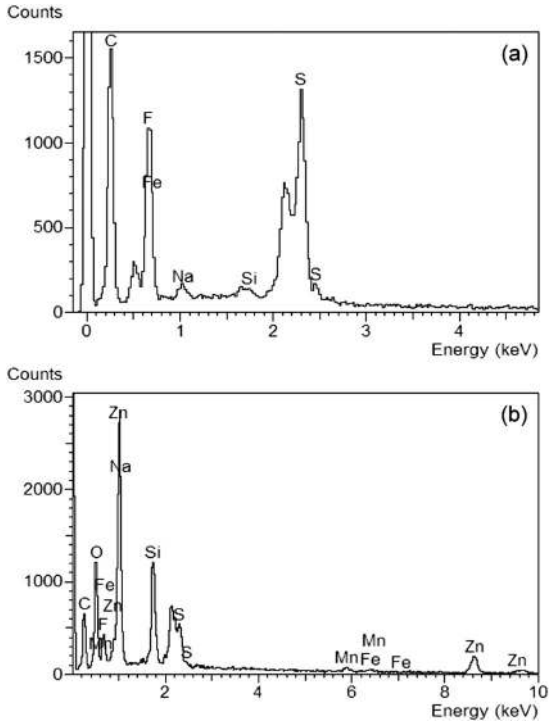

Fig. 3 EDX microanalysis spectra of: (a) sphere-like particles and (b) irregular-shaped microstructures.

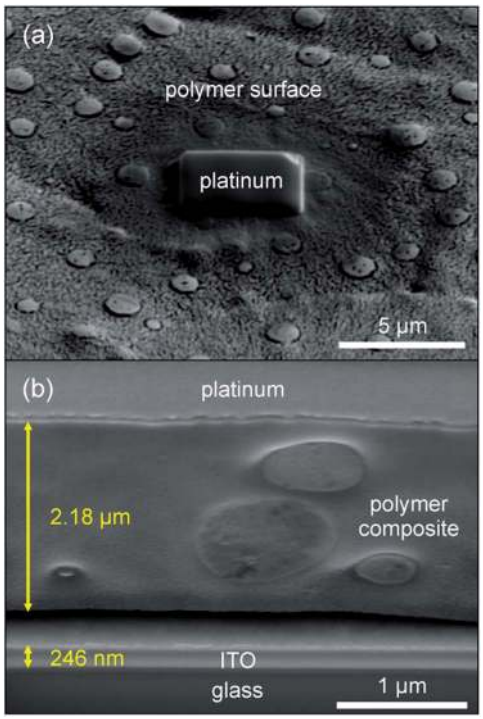

Fig. 4 FIB-SEM images of the sample prepared by the drop casting technique. (a) Overview of the region of the sample surface covered with platinum for the FIB milling process. (b) Cross-section of the region milled with the Ga^+ ion beam showing the Zn_2SiO_4:Mn and PT3MA microstructures embedded within the PVDF matrix.

particles (Fig. 3a) indicates the presence of carbon and sulphur, both constituents of the PT3MA polymer. Iron was also detected; the component of the ferric chloride used to dope the polymer. The irregular-shaped microstructures have also been probed. The EDX spectrum (Fig. 3b) shows that it is rich in zinc, silicon, manganese and oxygen – typical elements from the Zn_2SiO_4:Mn inorganic compound.

SEM images obtained using the FIB-SEM system (operating at 5 kV) are shown in Fig. 4. A region (approximately 5 μm × 3 μm) on the surface and near to one of the sample edges was covered with platinum (Fig. 4a). Subsequently, the metallized area, which acts as a protective layer, was milled with the Ga^+ ion beam. The acquired cross-sectional view image (such as Fig. 4b) refers to one of the walls of the rectangular hole produced by FIB milling. From the micrograph, it is interesting to notice that the Zn_2SiO_4:Mn and PT3MA microstructures not only are dispersed on the surface but also are buried in the PVDF matrix. Furthermore, a partial loss of adhesion of the polymeric composite to the ITO/glass substrate could be observed. This is mainly due to the local heating during the milling process, generated by energy transfer from the Ga ion beam to the sample.

The AFM technique was used to characterize the composite surface morphology in terms of roughness. For comparison purposes, 3D AFM images obtained from polymer layer surfaces deposited by spin-coating and drop casting are depicted in Fig. 5a and b, respectively. Protuberances are formed by spinner (visualized only on a nanometric height scale – Fig. 5a), but the roughness average is revealed to be lower with respect to drop casting. The profile roughness Sa parameter (arithmetic average of the 3D roughness) was found to be ≈11 nm (spin-coating) and ≈93 nm (drop casting) in an area of 10 × 10 μm^2. However, the spin coating method presents a drawback. AFM images of different surface areas indicate a substantial loss of PT3MA and

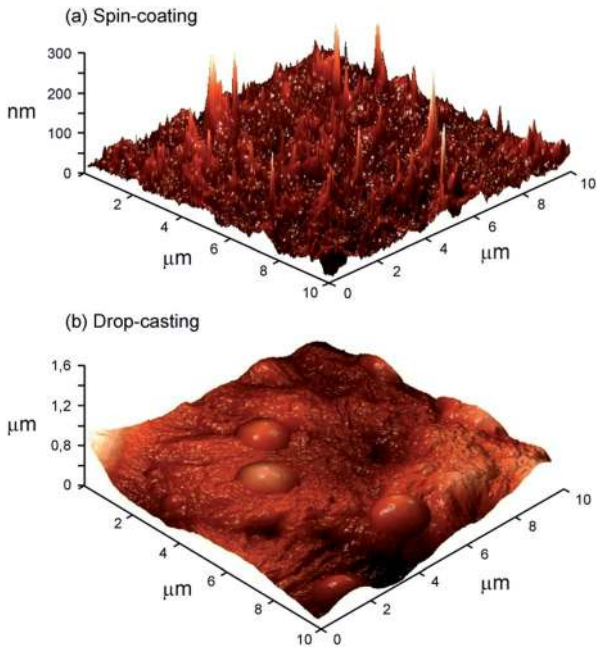

Fig. 5 3D AFM surface images of the polymeric layers deposited by (a) spin-coating at 2000 rpm and (b) drop casting.

of Zn_2SiO_4:Mn due to spreading during the substrate rotation. Although the surface became rougher, the drop casting proved to be the most appropriate technique. Moreover, a rougher film can make more efficient use of the excitation energy, since it enhances the excitation light that is reflected onto another part of the sample surface, resulting in better emission efficiency.[40]

Fig. 6 shows the current–voltage (*I–V*) characteristic curve of the fabricated device measured in the dark, whose curve exhibits a semiconductor behaviour typically observed for photodetectors.[41] The forward current values were approximately 3 times greater than the reverse current ones in an applied bias voltage range from −1 to +1 V. The dark leakage current, an important factor in the noise performance and detectivity of photodiode devices (shown in the inset of Fig. 6), at a reverse bias of −0.25 V was about 0.23 μA, while this value increased to 2.1 μA at −1 V. This increase in the leakage current might be due to the Al atoms that diffused from the electrodes to the polymer composite during the electrical contact deposition process. The diffused atoms result in leakage centres and trap centres for the charge carriers in addition to the large number of defects at the metal/polymer interface. This clearly illustrates the importance of interfacial engineering for performance enhancement of the device. Nevertheless, the electron injection from the negative electrode (cathode) can be improved. The strategy of incorporating an ionic dipole interlayer such as LiF (*i.e.*, between the active layer and the aluminium contact) has been used to enhance the performance of organic light-emitting devices fabricated by solution casting of polymers.[42]

The forward-bias *I–V* curve in the voltage range of 0 to 4 V, for larger currents (on the order of mA), is displayed in Fig. 7. For voltages greater than 3 V (currents > 2.8 mA), the device experienced a breakdown. We believe that this might have been caused by exceeded dissipated power, giving rise to a thermal breakdown and the beginning of the electrode rupture. From the result of Fig. 7, in the bias range between 1 and 3 V (more linear region), the resistance (924 Ω) and a DC electrical conductivity (σ_D) of approximately 0.37 μS cm^{-1} at 300 K were estimated. This conductivity value is in agreement with results

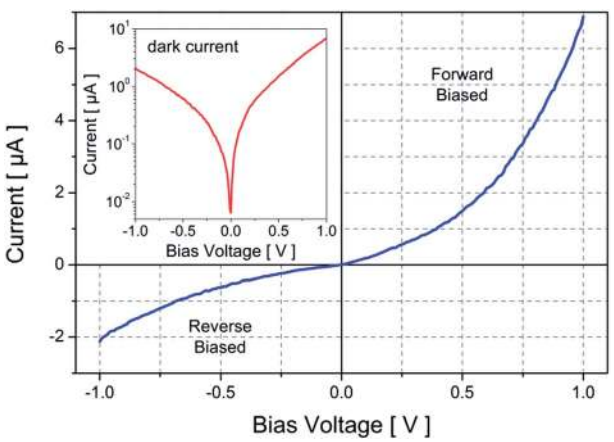

Fig. 6 Current–voltage characteristic curve measured in the dark at 300 K in an applied bias voltage range from −1 to +1 V.

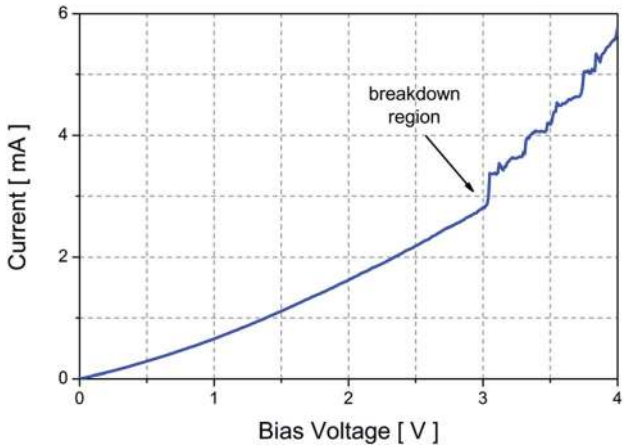

Fig. 7 Forward-bias *I–V* curve in the voltage range of 0 to 4 V for larger currents – order of mA.

previously obtained for other systems: poly(3-hexylthiophene) films, PT3MA:PE44 – poly(tetramethylene succinate) nanomembranes and PT3AA – poly(3-thiophene acetic acid) blends, all doped with $FeCl_3$.[31,33,43] Also, it is close to the order of magnitude of those reported ($\sim 10^{-5}$ S cm^{-1}) for alkyl 3,4-disubstituted polythiophenes: poly(3-octyl-4-methylthiophene), poly(3,4-dihexylthiophene) and poly(3,4-dibutoxylthiophene).[44] The charge transfer process across the polymer–metal interface as well as the conduction mechanism involved in the disordered system "insulating polymer/conducting polymer/inorganic phosphor" can be explained based on the tunneling[45] and hopping[46] phenomena, respectively.

Fig. 8 shows the spectral dependence of the optical absorption at room temperature of the ITO/glass substrate and of the PVDF–PT3MA–Zn_2SiO_4:Mn/ITO/glass multilayer structure, in the energy range between 1.55 and 6.43 eV (800–200 nm,

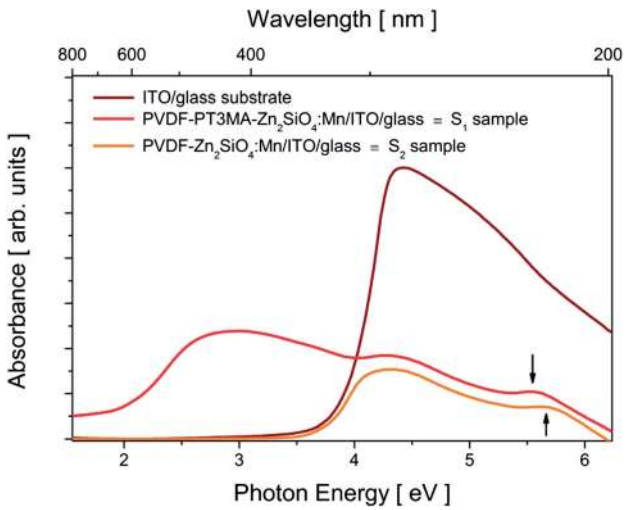

Fig. 8 UV-Vis optical absorbance spectra as a function of photon energy obtained at 300 K for the samples used in this work: ITO/glass substrate, PVDF–PT3MA–Zn_2SiO_4:Mn/ITO/glass and PVDF–Zn_2SiO_4:Mn/ITO/glass.

respectively). For comparative analysis, a PVDF–Zn_2SiO_4:Mn/ITO/glass sample (*i.e.*, without the PT3MA polymer) synthesized under the same conditions is also presented in Fig. 8. For convenience, from now on we call the PVDF–PT3MA–Zn_2SiO_4:Mn/ITO/glass sample as S_1 and the PVDF–Zn_2SiO_4:Mn/ITO/glass sample as S_2.

The UV-Vis absorbance spectrum of the polymeric composite with the PT3MA (S_1 sample) reveals absorption peaks at ≈5.53 eV (≈224 nm – corresponding to the optical band gap of Zn_2SiO_4),[10] at ≈4.43 eV (≈280 nm – assigned to the ITO/glass substrate),[47] and a broad band centred at ≈3 eV (≈410 nm – attributed to the π–π* transition of the thiophene ring of PT3MA).[30–32,48] The spectrum of the sample without PT3MA (S_2 sample) presents only the Zn_2SiO_4 and ITO/glass contributions. It is well known that PVDF does not exhibit significant absorption in the measured energy range. However, the absorption peak related to the zinc silicate lattice is slightly shifted (~112 meV) towards higher energy. The probable reason for this blue-shift is a change in the electronic structure due to the structural alterations, which should reflect in the light emission property.

PL investigation was undertaken using a 442 nm He–Cd laser for photoexcitation. This pump wavelength is not within the peak efficiency pumping (200–300 nm) found in PL excitation (PLE) spectra of the fixed 525 nm emission from Zn_2SiO_4:Mn.[10,49] The luminescence in the green range originates from the transition of the $3d^5$ electrons in the Mn^{2+} ions – from the transition between the lowest excited state and the ground state: $^4T_1(^4G) \rightarrow {}^6A_1(^6S)$ of tetrahedrally coordinated Mn.[50] In this case, the zinc silicate host lattice absorbs energy and transfers charge efficiently to Mn ions. However, Mn^{2+} ions can be directly excited in the wavelength range between 357 and 500 nm.[10,49] In particular, the 442 nm line (≈2.81 eV) is resonant with the $^4T_2(^4G)$ energy level.[50] From this level, the excited electrons can relax to the $^4T_1(^4G)$ state through non-radiative processes and then radiatively decay to the ground state. Therefore, the 442 nm is appropriate and also resonant with the PT3MA absorption peak.

PL spectra from the S_1 and S_2 samples, taken at 7 and at 295 K in the energy range between 1.46 and 2.76 eV (850–450 nm, respectively), are presented in Fig. 9. An intense broadband emission peaking at 2.365 eV (≈524.6 nm, better visualized in the inset), typical from Mn ions, is observed in the S_2 sample spectrum at 7 K. On the other hand at the same temperature, in the S_1 sample spectrum, the Mn^{2+} emission is found centred at 2.353 eV (≈527.3 nm) and superimposed by a considerably broad shoulder characteristic of the PT3MA polymer.[48] The emission from PT3MA is within the luminescence range (between 400 and 900 nm) typically found for polythiophene derivatives. The range of PL, from blue to red, is usually achieved by variations of the polythiophene structure *via* substituents at the 3,4-positions.[51,52]

The difference in the Mn emission peak position (about 12 meV) can be ascribed to the strength of the crystal field. In the Zn_2SiO_4 crystal, Mn^{2+} occupies part of the Zn^{2+} sites, which are coordinated by four oxygen atoms.[53,54] The weak crystal field around Mn^{2+} results in a low splitting width of its 3d energy

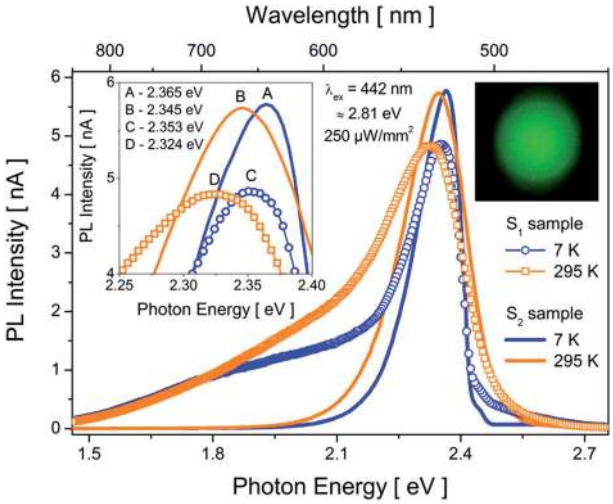

Fig. 9 PL spectra of the S_1 and S_2 samples at 7 and at 295 K: PVDF–PT3MA–Zn_2SiO_4:Mn/ITO/glass and PVDF–Zn_2SiO_4:Mn/ITO/glass, respectively. The insets show the rescaled spectra in the energy range of interest – Mn emission peak, and a digital camera image that represents emission colour as observed by the eyes under 442 nm violet pumping.

levels. The position of the luminescence band maximum is then influenced by the coordination environment. It is remarkable that the synthesis process with PVDF slightly impacts the crystal field surrounding Mn^{2+}. In fact, the crystal field becomes stronger and reduces the energy difference between the first excited and the ground state, resulting in the red-shift of the emission peak.[55,56] In other words, the Mn ions occupy higher symmetry sites. A further increase in the emission (about 1.2 times) is likely due to different spatial distributions of the optically active Mn centres in both samples. Concerning the PT3MA radiative transition from PL spectra, a Stokes shift (difference in energy between absorption and emission) of ≈1.1 eV was estimated, considering that the broadband is centred at 1.9 eV (≈650 nm).

At 295 K, the green emission varies, either in energy position or in bandwidth for the two samples. However, their intensity hardly depends on the temperature. Apparently, there is not PL thermal quenching, unlike the feature reported for Zn_2SiO_4:Mn particles embedded in a SiO_2 host matrix where the PL intensity decreases as the temperature increases.[57] Although the $^4T_1(^4G) \rightarrow {}^6A_1(^6S)$ optical transition is a localized transition within the $3d^5$ configuration of the Mn^{2+} ion, thermal effects such as carrier-phonon scattering give rise to intrinsic broadening of the band, as observed in the PL spectra at 295 K. The origin of the temperature-induced red shift, *i.e.*, the decrease in the transition energy is not completely understood. It would be expected that an increase of the temperature results in a decrease of the crystal field and a concomitant increase in the Mn^{2+} related emission energy; a blue-shift, contrary to the experimental result. However, it has been argued that exchange interactions between the Mn^{2+} ion pairs can be responsible for the red-shift of the emission.[58] Further investigations should be conducted to clarify this aspect.

It would be interesting to explore the hybrid composite as a photoactive layer for multi-coloured HyLEDs, since the PL covers a wide spectral range (500–800 nm). By applying different voltages, the control of fractions and intensities of the light emitted (tunable colours) can be obtained.[4,59] To accomplish this, improvements in the metallic cathode (electron injection) should be crucially implemented. Due to the rather low conductivity of the hybrid composite, charge conduction to achieve electroluminescence will require high electric fields and appropriate ohmic contacts. The possibility of the PT3MA polymer, as well as its hybrid composite, as a luminescence-based (bio) chemical sensor system for analytical applications in the fields of medicine, environment, defence and food needs to be investigated.[60–63]

Conclusions

The material synthesis, fabrication and characterization (morphological, electrical and optical) of a device based on a (PVDF–$FeCl_3$-doped PT3MA–Zn_2SiO_4:Mn) hybrid polymeric composite were presented. Recrystallized PVDF was used as a host matrix for the PT3MA polymer and Zn_2SiO_4:Mn inorganic compound. The hybrid composite was deposited on an indium-tin-oxide (ITO)-coated glass substrate by the drop casting technique to form an active layer. A spin-coating method was also used for morphological comparison purposes. AFM analyses showed that the composite layer obtained by drop casting is more appropriate for manufacture of the device than those produced by spin-coating, since by the latter there was a substantial loss of material due to spreading during the substrate rotation. In contrast, SEM images revealed that when films are obtained by drop casting both PT3MA and Zn_2SiO_4:Mn, in the form of microparticles, are dispersed on and within the PVDF matrix. Local chemical microanalyses by EDX allowed distinguishing the microstructures. UV-Vis absorbance spectra showed absorption peaks at $\approx$224 nm, which corresponds to the optical band gap of Zn_2SiO_4, and at $\approx$410 nm attributed to the π–π^* transition of the thiophene ring of the PT3MA. In the PL spectra, a strong broadband emission centred at $\approx$525 nm superimposed by a considerably broad shoulder (600–800 nm) was observed, originating from the Zn_2SiO_4:Mn radiative transitions and from the recombination of photogenerated carriers at PT3MA, respectively. Current–voltage (*I–V*) measurement of the device evaluated at room temperature in the dark has indicated a semiconducting behaviour, consistent with the photodetector character.

Finally, our preliminary findings demonstrated that the hybrid organic/inorganic composite is promising for application in UV-Vis photodetector devices. However, further investigations are required. The dependence of the decay process on the temperature as well as current–voltage (*I–V*) characteristic curves under illumination and the photoresponse and electroluminescence properties are being conducted as a function of the active layer thickness. These detailed analyses will be the subject of a forthcoming paper.

Acknowledgements

This work was partially supported by the Brazilian founding agencies CNPq, and Capes. Research of authors E. A. and C. A. was supported by MICINN and FEDER (MAT2012-34498) and Generalitat de Catalunya (Research Group 2009 SGR-925, XRQTC and prize "ICREA Academia" for excellence in research to C. A.). One of the authors (A. L. G.) also acknowledges the financial support from the Euro Brazilian Windows agency (grant no. 41309-EM-1-2008-PT-ERAMUNDUS-ECW-L16). The authors are also grateful to J. G. of the Arkema Inc. (Philadelphia, USA) for supplying Kynar 740 pellets and at the Center of Semiconductor Components (UNICAMP, Campinas, Brazil) for the AFM and FIB-SEM measurements and technical support.

References

1 C. Sanchez, B. Julián, P. Belleville and M. Popall, *J. Mater. Chem.*, 2005, **15**, 3559–3592.
2 S. A. Mcdonald, G. Konstantatos, S. Zhang, P. W. Cyr, E. J. D. Klem, L. Levina and E. H. Sargent, *Nat. Mater.*, 2005, **4**, 138–142.
3 H. J. Bolink, H. Brine, E. Coronado and M. Sessolo, *Adv. Mater.*, 2010, **22**, 2198–2201.
4 M. Sessolo and H. J. Bolink, *Adv. Mater.*, 2011, **23**, 1829–1845.
5 N. Tokmoldin, N. Griffiths, D. D. C. Bradley and S. A. Haque, *Adv. Mater.*, 2009, **21**, 3475–3478.
6 M. Sessolo, H. J. Bolink, H. Brine, H. Prima-Garcia and R. Tena-Zaera, *J. Mater. Chem.*, 2012, **22**, 4916–4920.
7 D. C. Choo, S. D. Ahn, H. S. Jung, T. W. Kim, J. Y. Lee, J. H. Park and M. S. Kwon, *Thin Solid Films*, 2010, **518**, 6308–6310.
8 S. C. Allen and A. J. Steckl, *Appl. Phys. Lett.*, 2008, **92**, 143309.
9 G. Gozzi, D. L. Chinaglia, T. F. Schmidt and O. N. Oliveira Jr, *Mater. Sci. Eng., C*, 2011, **31**, 969–974.
10 A. Morell and N. El Khiati, *J. Electrochem. Soc.*, 1993, **140**, 2019–2022.
11 C. R. Ronda, *J. Lumin.*, 1997, **72–74**, 49–54.
12 T. Miyata, T. Minami, K. Saikai and S. Takata, *J. Lumin.*, 1994, **60–61**, 926–929.
13 R. Ye, G. Jia, D. Deng, Y. Hua, Z. Cui, S. Zhao, L. Huang, H. Wang, C. Li and S. Xu, *J. Phys. Chem. C*, 2011, **115**, 10851–10858.
14 W. U. Huynh, J. J. Dittmer and A. P. Alivisatos, *Science*, 2002, **295**, 2425–2427.
15 E. Arici, N. S. Sariciftci and D. Meissner, *Adv. Funct. Mater.*, 2003, **13**, 165–171.
16 R. Thapa, K. R. Choudhury, W. J. Kim, Y. Sahoo, A. N. Cartwright and P. N. Prasad, *Appl. Phys. Lett.*, 2007, **90**, 252112.
17 D. M. N. M. Dissanayake, R. A. Hatton, T. Lutz, C. E. Giusca, R. J. Curry and S. R. P. Silva, *Appl. Phys. Lett.*, 2007, **91**, 133506.
18 T. K. An, C. E. Park and D. S. Chung, *Appl. Phys. Lett.*, 2013, **102**, 193306.
19 Y. Han, C. Fan, G. Wu, H. Chen and M. Wang, *J. Phys. Chem. C*, 2011, **115**, 13438–13445.

20 T. Yang, K. Sun, X. Liu, W. Wei, T. Yu, X. Gong, D. Wang and Y. Cao, *J. Phys. Chem. C*, 2012, **116**, 13650–13653.
21 F. Guo, B. Yang, Y. Yuan, Z. Xiao, Q. Dong, Y. Bi and J. Huang, *Nat. Nanotechnol.*, 2012, **7**, 798–802.
22 T. A. Skotheim and J. R. Reynolds, *Handbook of Conducting Polymers*, CRC, Taylor and Francis, Boca Raton, 3rd edn, 2007.
23 G. G. Wallace, G. M. Spinks, L. A. P. Kane-Maguire and P. R. Teasdale, *Conductive Electroactive Polymers*, CRC, Taylor and Francis, Boca Raton, 3rd edn, 2009.
24 R. D. McCullough, *Adv. Mater.*, 1998, **10**, 93–116.
25 M. R. Anderson, O. Thomas, W. Mammo, M. Svensson, M. Theander and O. Inganäs, *J. Mater. Chem.*, 1999, **9**, 1933–1940.
26 H. Dong, H. Zhu, Q. Meng, X. Gong and W. Hu, *Chem. Soc. Rev.*, 2012, **41**, 1754–1808.
27 D. C. Basset, *Developments in Crystalline Polymers*, Applied Science Publishers, London, 1982, vol. 1.
28 G. Botelho, S. Lanceros-Mendez, A. M. Gonçalves, V. Sencadas and J. G. Rocha, *J. Non-Cryst. Solids*, 2008, **354**, 72–78.
29 O. Bertran, E. Armelin, F. Estrany, A. Gomes, J. Torras and C. Alemán, *J. Phys. Chem. B*, 2010, **114**, 6281–6290.
30 A. L. Gomes, J. Casanovas, O. Bertran, J. S. C. Campos, E. Armelin and C. Alemán, *J. Polym. Res.*, 2011, **18**, 1509–1517.
31 E. Armelin, A. L. Gomes, M. M. Pérez-Madrigal, J. Puiggalí, L. Franco, L. J. Del Valle, A. Rodríguez-Galán, J. S. C. Campos, N. Ferrer-Anglada and C. Alemán, *J. Mater. Chem.*, 2012, **22**, 585–594.
32 A. L. Gomes, M. B. P. Zakia, J. G. Filho, E. Armelin, C. Alemán and J. S. C. Campos, *Polym. Chem.*, 2012, **3**, 1334–1343.
33 R. K. Singh, J. Kumar, R. Singh, R. Kant, R. C. Rastogi, S. Chand and V. Kumar, *New J. Phys.*, 2006, **8**, 112.
34 J. Kumar, R. K. Singh, S. Chand, V. Kumar, R. C. Rastogi and R. Singh, *J. Phys. D: Appl. Phys.*, 2006, **39**, 196–202.
35 R. Sugimoto, S. Takeda, H. B. Gu and K. Yoshino, *Chem. Express*, 1986, **1**, 635–638.
36 B. S. Kim, L. Chen, J. Gong and Y. Osada, *Macromolecules*, 1999, **32**, 3964–3969.
37 G. Bradshaw and A. H. Hughes, *Thin Solid Films*, 1976, **33**, L5–L7.
38 J. S. Kim, M. Granström, R. H. Friend, N. Johansson, W. R. Salaneck, R. Daik, W. J. Feast and F. Cacialli, *J. Appl. Phys.*, 1998, **84**, 6859–6870.
39 J. Bao, C. C. Xu and W. Cai, *J. Appl. Polym. Sci.*, 1994, **52**, 1489–1497.
40 M. Cich, K. Kim, H. Choi and S. T. Hwang, *Appl. Phys. Lett.*, 1998, **73**, 2116–2118.
41 Y. Han, G. Wu, M. Wang and H. Chen, *Polymer*, 2010, **51**, 3736–3743.
42 T. M. Brown, R. H. Friend, I. S. Millard, D. J. Lacey, J. H. Burroughes and F. Cacialli, *Appl. Phys. Lett.*, 2000, **77**, 3096–3098.
43 K. H. Hsieh, K. S. Ho, Y. Z. Wang, S. D. Ko and S. C. Fu, *Synth. Met.*, 2001, **123**, 217–224.
44 M. Leclerc and G. Daoust, *J. Chem. Soc., Chem. Commun.*, 1990, **3**, 273–274.
45 I. D. Parker, *J. Appl. Phys.*, 1994, **75**, 1656–1666.
46 J. C. Dyre, *J. Appl. Phys.*, 1988, **64**, 2456–2468.
47 S. Kundu and P. K. Biswas, *Chem. Phys. Lett.*, 2005, **414**, 107–110.
48 S. Manna, A. Mandal and A. K. Nandi, *J. Phys. Chem. B*, 2010, **114**, 2342–2352.
49 K.-S. Sohn, B. Cho and H. D. Park, *J. Am. Ceram. Soc.*, 1999, **82**, 2779–2784.
50 D. T. Palumbo and J. J. Brown Jr, *J. Electrochem. Soc.*, 1970, **117**, 1184–1188.
51 I. F. Perepichka, D. F. Perepichka, H. Meng and F. Wudl, *Adv. Mater.*, 2005, **17**, 2281–2305.
52 L. Akcelrud, *Prog. Polym. Sci.*, 2003, **28**, 875–962.
53 H. K. Perkins and M. J. Sienko, *J. Chem. Phys.*, 1967, **46**, 2398–2401.
54 M. Takesue, H. Hayashi and R. L. Smith Jr, *Prog. Cryst. Growth Charact. Mater.*, 2009, **55**, 98–124.
55 J. Wan, Z. Wang, X. Chen, L. Mu, W. Yu and Y. Qian, *J. Lumin.*, 2006, **121**, 32–38.
56 G. Blasse and B. C. Grabmaier, *Luminescent Materials*, Springer-Verlag, 1994, pp. 20–25.
57 J. El Ghoul, C. Barthou, M. Saadoun and L. El Mir, *Phys. B*, 2010, **405**, 597–601.
58 C. R. Ronda and T. Amrein, *J. Lumin.*, 1996, **69**, 245–248.
59 K. Nakamura, T. Ishikawa, D. Nishioka, T. Ushikubo and N. Kobayashia, *Appl. Phys. Lett.*, 2010, **97**, 193301.
60 K. S. Nalwa, Y. Cai, A. L. Thoeming, J. Shinar, R. Shinar and S. Chaudhary, *Adv. Mater.*, 2010, **22**, 4157–4161.
61 C. Zanardi, F. Terzi and R. Seeber, *Anal. Bioanal. Chem.*, 2013, **405**, 509–531.
62 Z. Yao, C. Li and G. Shi, *Langmuir*, 2008, **24**, 12829–12835.
63 B. Adhikari and S. Majumdar, *Prog. Polym. Sci.*, 2004, **29**, 699–766.